DAXX directs dual modes of H3.4-to-H3.3 histone replacement in the male germline

Yu-Han Yeh,[1] Mengwen Hu,[1,3] Kai Otsuka,[2] Brooke M. Alger,[1] Shruti S. Nene,[1] Han Wang,[1] So Maezawa,[2] and Satoshi H. Namekawa[1]

[1]Department of Microbiology and Molecular Genetics, University of California, Davis, Davis, California 95616, USA; [2]Department of Applied Biological Science, Faculty of Science and Technology, Tokyo University of Science, Noda, Chiba 281-8510, Japan

During spermatogenesis, extensive chromatin remodeling and histone replacement reshape the male germline epigenome. Although HIRA mediates transcription-coupled incorporation of histone variant H3.3, we identified DAXX as a key histone chaperone directing genome-wide, transcription-coupled replacement of H3.4 (H3T) with H3.3 on autosomes during male meiosis. Simultaneously, DAXX also directs transcription-independent H3.4-to-H3.3 replacement on the sex chromosomes during meiotic sex chromosome inactivation (MSCI). These distinct, chromosome-specific modes of DAXX-mediated H3.3 deposition are essential for epigenomic integrity in the male germline. Loss of DAXX disrupts this process, resulting in widespread transcriptional dysregulation in haploid round spermatids and impaired male fertility.

Supplemental material is available for this article.

Received October 11, 2025; revised version accepted January 8, 2026.

Nucleosome deposition and remodeling are critical processes during DNA replication, repair, transcription, and epigenetic gene regulation. Histone H3, a core nucleosome component, exists in several variant forms in the mammalian genome. While the canonical histones H3.1 and H3.2 are incorporated in a replication-dependent manner, the variant H3.3 is deposited independently of DNA replication (Tagami et al. 2004). At gene regulatory elements and promoters, H3.3 incorporation is mediated primarily by the histone chaperone HIRA (Ray-Gallet et al. 2002), implicating H3.3 in transcriptional activation. In contrast, the chaperone DAXX deposits H3.3 into heterochromatin regions, including telomeres and retrotransposons (Lewis et al. 2010; Elsässer et al. 2015), suggesting a repressive function for H3.3 in these contexts (Choi et al. 2024). In the germline, HIRA-dependent H3.3 incorporation is essential for early embryogenesis (Lin et al. 2014) and oogenesis (Nashun et al. 2015), whereas DAXX-mediated H3.3 deposition is crucial for maintaining genome integrity and embryonic heterochromatin (Liu et al. 2020). Despite these insights, how H3.3 deposition is regulated in the male germline remains a fundamental unanswered question, particularly during spermatogenic differentiation, a process marked by massive H3.3 incorporation (van der Heijden et al. 2007; Erkek et al. 2013).

During spermatogenesis, one prominent feature of nucleosome dynamics is the replication-dependent incorporation of the testis-specific variant H3.4 (also known as H3T) during the mitotic proliferation of differentiating spermatogonia (Ueda et al. 2017). As differentiation progresses, canonical H3.1 and H3.2 are gradually replaced by H3.4. Subsequent incorporation of H3.3 during later stages of spermatogenesis implies extensive replacement of H3.4 by H3.3. Here we identify a dual role for DAXX in this process: DAXX mediates transcription-coupled H3.4-to-H3.3 replacement on autosomes and transcription-independent replacement on the sex chromosomes during meiotic sex chromosome inactivation (MSCI). This coordinated histone exchange is essential for maintaining the epigenetic integrity necessary for male fertility and may also serve to bookmark the sperm epigenome for epigenetic inheritance.

Results and Discussion

DAXX deletion compromised spermatogenesis

During spermatogenesis, H3.3 is incorporated into the promoters of autosomal genes that are rich in CpG sites (Erkek et al. 2013). A chromosome-wide incorporation of H3.3 also occurs on the sex chromosome during MSCI (van der Heijden et al. 2007), a process essential for spermatogenesis (Fig. 1A; Turner 2015; Alavattam et al. 2021). Analysis of RNA-seq data sets for germ cell development and spermatogenesis revealed that the *Daxx* transcript is highly expressed during male meiosis, whereas the *Hira* transcript is downregulated at this stage (Fig. 1B). Consistent with a previous report (Rogers et al. 2004), we confirmed that DAXX accumulates on the XY body (a transcriptionally silent nuclear compartment formed during MSCI), marked by a key DNA damage response (DDR) marker: phosphorylated S139 of the histone variant H2AX (γH2AX) (Fig. 1C).

To investigate the function of DAXX in male germ cells, we generated *Daxx* conditional knockout (*Daxx*-cKO) mice by crossing mice carrying a floxed *Daxx* allele with those harboring the germ cell-specific *Ddx4*-Cre transgene, which is expressed from embryonic day 15 (E15) (Supplemental Fig. S1A; Gallardo et al. 2007). *Daxx*-cKO male mice exhibited significantly smaller testes and a

[*Keywords*: spermatogenesis; meiosis; meiotic sex chromosome inactivation; DAXX; histone chaperone]

[3]Present address: Guangzhou Key Laboratory of Metabolic Diseases and Reproductive Health, Guangdong-Hong Kong Metabolism and Reproduction Joint Laboratory, Reproductive Medicine Center, The Affiliated Guangdong Second Provincial General Hospital of Jinan University, Guangzhou 510317, China.

Corresponding author: snamekawa@ucdavis.edu

Article published online ahead of print. Article and publication date are online at http://www.genesdev.org/cgi/doi/10.1101/gad.353435.125. Freely available online through the *Genes & Development* Open Access option.

© 2026 Yeh et al. This article, published in *Genes & Development*, is available under a Creative Commons License (Attribution-NonCommercial 4.0 International), as described at http://creativecommons.org/licenses/by-nc/4.0/.

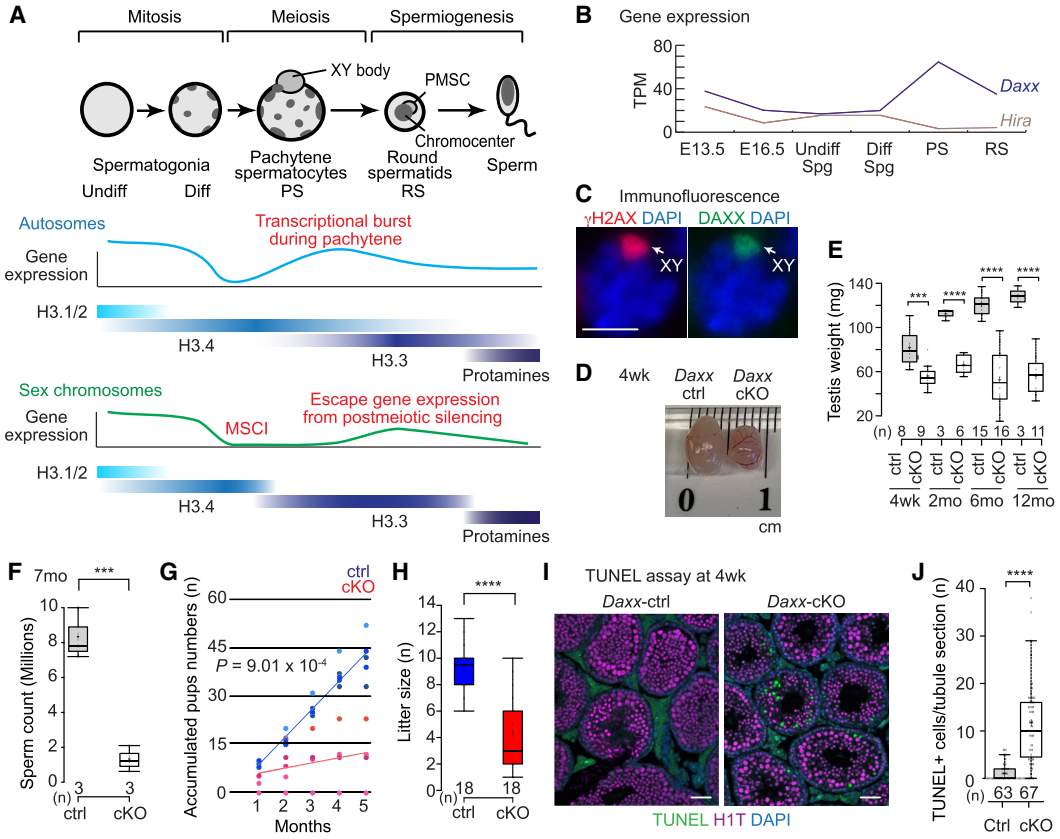

Figure 1. DAXX deletion compromises spermatogenesis. (*A*) Schematic of mouse spermatogenesis, illustrating gene expression levels and histone profiles on autosomes and sex chromosomes. (MSCI) Meiotic sex chromosome inactivation, (PMSC) postmeiotic sex chromatin. (*B*) Gene expression profiles of *Daxx* and *Hira* during spermatogenesis. (E13.5) Male germ cells at E13.5, (E16.5) male germ cells at E16.5, (Undiff Spg) P7 THY1$^+$ undifferentiated spermatogonia, (Diff Spg) P7 cKIT$^+$ differentiating spermatogonia, (PS) pachytene spermatocytes, (RS) round spermatids. (*C*) Immunofluorescence image of a pachytene spermatocyte in a testicular section. Scale bar, 5 µm. (XY) XY body. (*D*) Testes from *Daxx*-ctrl and *Daxx*-cKO mice at 4 weeks of age. Scale shown is 1 cm. (*E*) Whisker plots showing testis weights for *Daxx*-ctrl and *Daxx*-cKO males. The number of independent mice analyzed is indicated *below*. The central line represents the median, and the upper and lower hinges correspond to the 25th and 75th percentiles, respectively. *P*-values are from pairwise *t*-tests. (***) $P < 0.001$, (****) $P < 0.0001$. (*F*) Sperm counts for *Daxx*-ctrl and *Daxx*-cKO males at 7 months of age. The number of independent mice analyzed is indicated *below*. Whisker plots are as described in *E*. *P*-values are from pairwise *t*-tests. (***) $P < 0.001$. (*G*) Cumulative number of pups sired by *Daxx*-ctrl and *Daxx*-cKO males. Five independent male mice were analyzed for each group. (*H*) Litter sizes from live births sired by *Daxx*-ctrl and *Daxx*-cKO males. Whisker plots are as described in *E*. *P*-values are from pairwise *t*-tests. (****) $P < 0.0001$. (*I*) TUNEL assay combined with immunofluorescence for H1T in testicular sections at 4 weeks of age. Scale bars, 10 µm. (*J*) TUNEL-positive cells per tubule section. The number of tubules analyzed is indicated *below*. Three independent mice were analyzed. Whisker plots are as described in *E*. *P*-values are from pairwise *t*-tests. (****) $P < 0.0001$.

marked reduction in sperm count compared with controls (Fig. 1D–F). Fertility was also compromised in *Daxx*-cKO males: While young males (2 months old) were initially able to sire a small number of pups within the first 3 months of breeding, older males became infertile (Fig. 1G). Among live births, litter sizes sired by *Daxx*-cKO males were significantly smaller than those of littermate controls (Fig. 1H), and we confirmed transmission of the mutant alleles to the offspring. Immunostaining of spermatocytes revealed the absence of DAXX on the XY body in *Daxx*-cKO testes, confirming efficient depletion via Cre-mediated recombination (Supplemental Fig. S1B). Additionally, seminiferous tubules in *Daxx*-cKO testes were reduced in size and showed an increased proportion of apoptotic cells and abnormal tubules, often lacking round spermatids (RSs) and exhibiting germ cell depletion, with germ cell reduction most evident at the RS stage (Fig. 1I,J; Supplemental Fig. S1C–F). The epididymides of *Daxx*-cKO males contained fewer spermatozoa, with numbers declining with age, and the remaining sperm often exhibited abnormal morphology, including folded tails, headless sperm, or double-headed sperm (Supplemental Fig. S1G,H). *Daxx*-cKO spermatozoa lacked motility at 6 months of age (Supplemental Fig. S1I; Supplemental Videos S1, S2). Together, these findings demonstrate that DAXX is a critical regulator of spermatogenesis.

DAXX regulates H3.4-to-H3.3 histone replacement on meiotic sex chromosomes

To investigate the role of DAXX in male meiosis, we examined the meiotic phenotype of *Daxx*-cKO male mice. Notably, H3.3 incorporation on the XY body was absent in testicular sections, while H3.4 accumulated prominently (Fig. 2A–C), indicating that DAXX directs the replacement of H3.4 with H3.3 on the XY chromatin. A

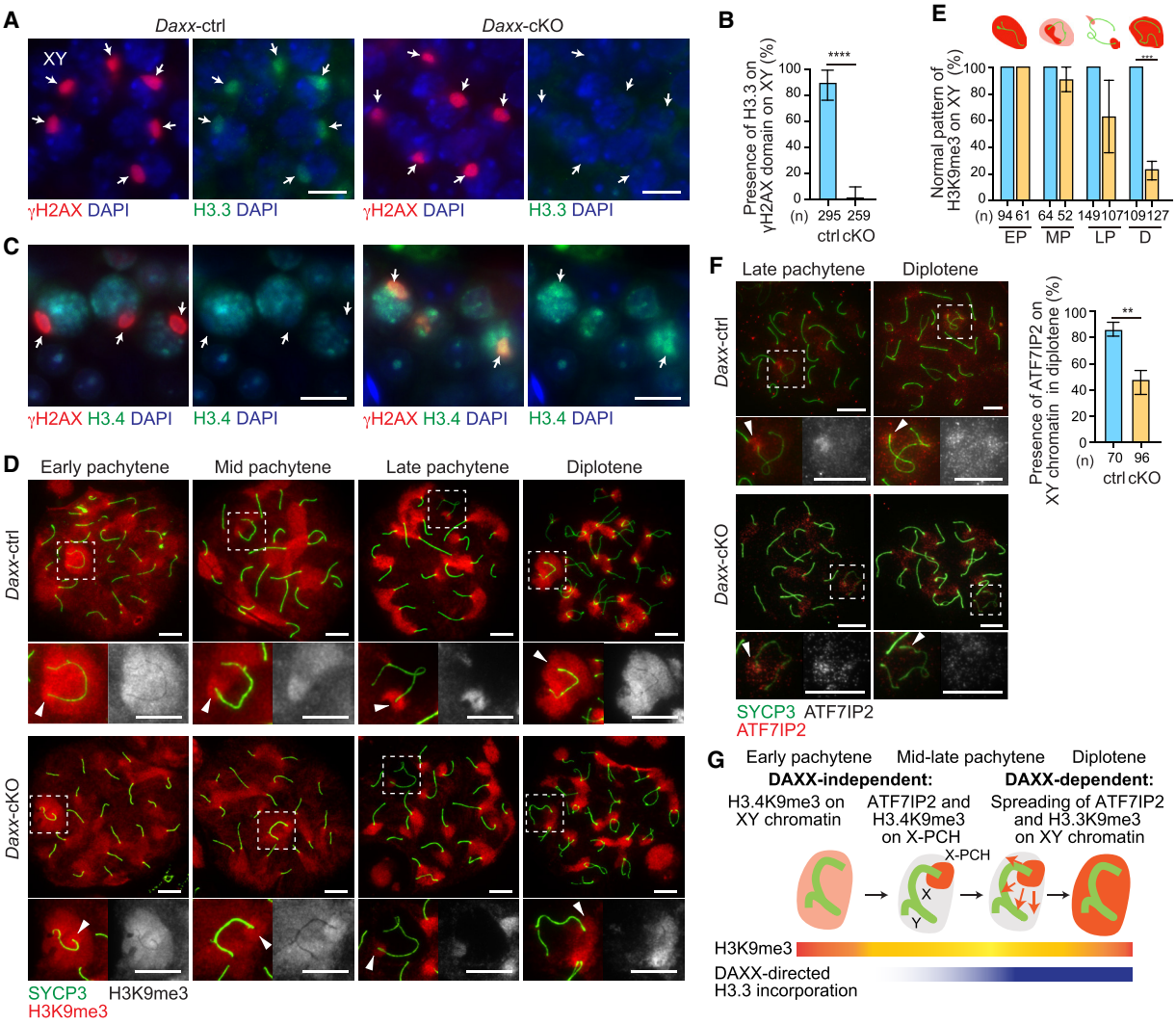

Figure 2. DAXX-deposited H3.3 is required for H3K9me3 establishment on the sex chromosomes. (*A*,*C*) Immunofluorescence images of pachytene spermatocytes in testicular sections. Scale bars, 10 µm. Arrows indicate XY bodies (XY). (*B*) Quantification of H3.3$^+$ domain presence per γH2AX$^+$ XY body. The number of cells analyzed from three independent mice is indicated *below*. Data are presented as mean ± SD from three independent mice. *P*-values are from pairwise *t*-tests. (****) $P < 0.0001$. (*D*,*F*, *left*) Immunofluorescence images of pachytene spermatocytes on chromosome spreads. Dashed squares on XY bodies are magnified *below*. Scale bars, 10 µm. Arrowheads indicate X pericentromeric heterochromatin (X-PCH). (*F*, *right*) Quantification of ATF7IP2 presence per XY body. The number of cells analyzed from three independent mice is indicated *below*. Data are presented as mean ± SD from three independent mice. *P*-values are from pairwise *t*-tests. (**) $P < 0.01$. (*E*) Proportion of pachytene substages showing a normal H3K9me3 pattern on XY bodies. The schematic *above* represents normal accumulation patterns. (EP) Early pachytene, (MP) mid-pachytene, (LP) late pachytene, (D) diplotene. The number of cells analyzed from three independent mice is indicated *below*. Data are presented as mean ± SD from three independent mice. *P*-values are from pairwise *t*-tests. (***) $P < 0.001$. (*G*) Summary of DAXX-independent ATF7IP2 and H3K9me3 localization on X-PCH and DAXX-dependent spreading of ATF7IP2 and H3K9me3 on XY chromatin.

hallmark of the XY body is the histone modification H3K9me3, which undergoes dynamic regulation during MSCI (van der Heijden et al. 2007). In early pachytene spermatocytes (PSs), H3K9me3 is established across the entire sex chromosome chromatin (Fig. 2D). During the mid-pachytene stage, coinciding with histone replacement, H3K9me3 signals decrease on the X chromosome and become restricted to the X pericentromeric heterochromatin (X-PCH) in late pachytene, before being re-established across XY chromatin in diplotene (Fig. 2D). In *Daxx*-cKO spermatocytes, H3K9me3 persisted on X-PCH, though its intensity was reduced, and failed to spread across XY chromatin in diplotene (Fig. 2D,E), suggesting a critical role for DAXX in this process.

The methyltransferase SETDB1 mediates formation of H3K9me3 on the XY chromosomes during MSCI (Hirota et al. 2018; Abe et al. 2022), and the re-establishment of H3K9me3 on XY chromatin from late pachytene to diplotene requires the germline-specific cofactor ATF7IP2/MCAF2 (Shao et al. 2023; Alavattam et al. 2024). In *Daxx*-cKO spermatocytes, ATF7IP2 intensity at X-PCH was reduced at the late pachytene stage, and chromosome-wide spreading of ATF7IP2 was largely diminished at the diplotene stage (Fig. 2F), demonstrating that DAXX regulates ATF7IP2 loading and the subsequent re-establishment of H3K9me3 on XY chromatin at the diplotene stage. These results suggest that H3.4-based H3K9me3 is removed from the XY chromatin but retained

at X-PCH and that, following H3.3 incorporation, H3.3-based H3K9me3 spreads to the XY chromatin during diplotene (Fig. 2G). Because DAXX can facilitate the generation of H3.3K9me3 on newly synthesized H3.3–H4 dimers prior to nucleosome deposition (Carraro et al. 2023), it is conceivable that DAXX promotes ATF7IP2–SETDB1-mediated formation of H3.3K9me3 before incorporation into XY chromatin, thereby ensuring proper histone modification during MSCI.

DAXX distinctively mediates H3.4-to-H3.3 histone replacement between autosomes and sex chromosomes

To examine how DAXX regulates H3.4-to-H3.3 replacement and H3K9me3 deposition, we performed CUT&RUN on *Daxx*-ctrl and *Daxx*-cKO PSs for H3.1/3.2, H3.3, H3.4, H3K9me3, and H3K27ac, an active enhancer/promoter mark enriched in PSs (Supplemental Fig. S2A,B; Adams et al. 2018; Maezawa et al. 2020). H3.3 deposition on both autosomes and sex chromosomes was largely DAXX-dependent, with particularly strong enrichment at autosomal transcription start sites (TSSs)/promoters and at intergenic regions of the sex chromosomes compared with their expected genomic distribution (Fig. 3A,B). In contrast, H3.4 was retained in *Daxx*-cKO PSs. Despite the DAXX-dependent shift from H3.4 to H3.3, we did not detect major DAXX-dependent changes in H3.1/3.2 (Supplemental Fig. S2C). Broad H3K9me3 accumulation on sex chromosomes was also DAXX-dependent (Fig. 3A), reflecting DDR-directed chromosome-wide regulation by ATF7IP2 and SETDB1 (Hirota et al. 2018; Abe et al. 2022; Alavattam et al. 2024). In addition, H3K27ac accumulation at TSSs on both autosomes and sex chromosomes was largely attenuated in *Daxx*-cKO PSs, which is primarily attributable to the loss of H3.3, as DAXX-dependent H3.3 incorporation coincides with H3K27ac peaks (Supplemental Fig. S2D).

Clustering analysis of autosomal genes revealed that H3.3 is highly deposited at actively transcribed genes (clusters 1–3), whereas genes expressed at a low level or not expressed (cluster 4) showed minimal H3.3 deposition

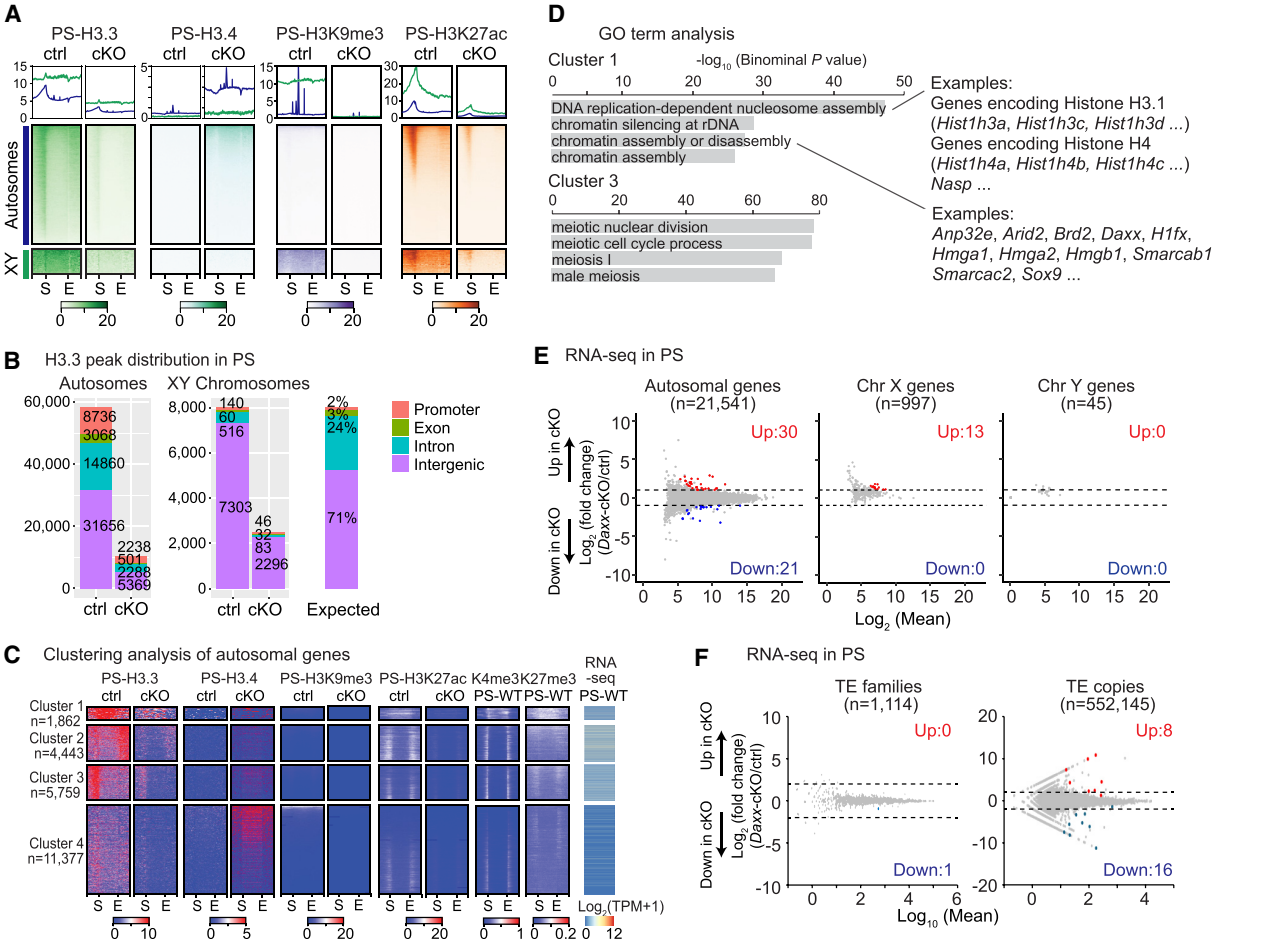

Figure 3. DAXX distinctively mediates H3.4-to-H3.3 replacement between autosomes and sex chromosomes. (*A*) CUT&RUN enrichment profiles of H3.3, H3.4, H3K9me3, and H3K27ac at all autosomal genes ($n = 23,441$) and all XY-linked genes ($n = 1324$). (S) TSS, (E) TES; ±3 kb from these sites. (*B*) Number and genomic distribution of H3.3 CUT&RUN peaks on autosomes and sex chromosomes in PSs. The expected distribution is shown at the *right*. (*C*) Clustering analysis based on H3.3 and H3.4 enrichment in *Daxx*-ctrl and *Daxx*-cKO PSs. (*D*) Gene ontology (GO) term analysis of clusters 1 and 3, with representative genes indicated. (*E*) RNA-seq analysis of *Daxx*-ctrl and *Daxx*-cKO PSs. DEGs ($\log_2$ fold change >1, adjusted $P < 0.05$) are highlighted, with numbers shown. (*F*) Differential expression analysis of TEs at both family and copy levels in *Daxx*-ctrl and *Daxx*-cKO PSs (adjusted $P < 0.05$). DE TEs are colored, with numbers indicated.

in *Daxx*-ctrl PSs and retention of H3.4 in *Daxx*-cKO PSs (Fig. 3C). Thus, on autosomes, DAXX mediates transcription-coupled H3.3 incorporation. Notably, H3.3 deposition extended from TSSs into gene bodies in cluster 1 genes, which also displayed features of bivalent chromatin, with concurrent enrichment of active marks (H3K4me3 and H3K27ac) and the repressive H3K27me3 mark. Cluster 1 genes include intron-less histone genes encoding H3.1 and H4, as well as genes involved in nucleosome and chromatin assembly/disassembly, such as histone chaperones (*Nasp*, *Anp32e*, and *Daxx*) and chromatin remodelers (*Arid2*, *Brd2*, and *Smarcab1*) (Fig. 3D). In cluster 2 genes, H3.3 was enriched downstream from TESs, while in cluster 3 genes, it was enriched upstream of TSSs, encompassing genes involved in meiosis.

Despite these chromatin changes, RNA sequencing (RNA-seq) analysis revealed only minor alterations in autosomal gene expression, with 30 genes upregulated and 21 downregulated, along with modest upregulation of 13 X-linked genes (Fig. 3E; Supplemental Fig. S2E; Supplemental Table S1). DAXX did not regulate H3.3 at the transcriptional level, as RNA-seq reads at the *H3f3a* and *H3f3b* gene loci, which encode the H3.3 transcript, remained unchanged upon *Daxx* deletion (Supplemental Fig. S2F). Additionally, we did not observe major changes in transposable element (TE) expression across families or copies, in contrast to a recent study (Fig. 3F; Supplemental Table S2; Li et al. 2026). Together, these results indicate that DAXX mediates transcription-coupled H3.3 deposition, but this process does not substantially affect autosomal gene expression in PSs. In contrast, on sex chromosomes, DAXX directs transcription-independent H3.3 deposition downstream from DDR signaling during MSCI.

DAXX-mediated H3.3 deposition in PSs sets up a proper epigenome in RSs

After completion of meiotic prophase I, the XY body gives rise to a silent chromatin compartment of either the X or Y chromosome, termed postmeiotic sex chromatin (PMSC), in postmeiotic RSs (Namekawa et al. 2006). In *Daxx*-cKO RSs, H3.3 signals reappeared on the PMSC but remained lower than in *Daxx*-ctrl RSs (Fig. 4A; Supplemental Fig. S3A), suggesting partial recovery of H3.3. CUT&RUN analysis further confirmed this recovery on autosomes, though H3.3 levels remained reduced compared with controls (Fig. 4B; Supplemental Fig. S3B). Using the same clusters defined in Figure 3C, we found that H3.3-enriched sites on autosomes in RSs were largely consistent with those in PSs (Fig. 4C). This finding indicates that DAXX-dependent H3.3 incorporation in PSs predetermined H3.3 deposition sites in RSs, a subset of which was recovered independently of DAXX. Despite the attenuated H3.3 incorporation in *Daxx*-cKO RSs, levels of H3K9me3 and H3K27ac were increased relative to controls, which could be attributable to retained H3.4. Taken together, proper H3.3 incorporation in PSs is a prerequisite for establishing an appropriate epigenome in RSs. One possible explanation for the increased levels of these histone marks despite reduced H3.3 is their ectopic deposition on nucleosomes lacking H3.3.

In *Daxx*-cKO RSs, substantial changes in gene expression were observed: 1049 genes were upregulated, while 1943 genes were downregulated (Fig. 4D; Supplemental Table S1; Supplemental Fig. S3C). The upregulated genes are typically highly expressed in RSs, whereas the downregulated genes are normally repressed (Supplemental Fig. S3D), suggesting that the DAXX-directed epigenome is required to maintain appropriate gene expression levels in RSs. Furthermore, key apoptosis-related genes were upregulated in *Daxx*-cKO RSs (Fig. 4E), consistent with the increased apoptotic cell death observed (Fig. 1I,J). Expression of the alternative H3.3 chaperone *Hira* was not upregulated in *Daxx*-cKO RSs (Supplemental Table S1), suggesting that HIRA does not compensate for the loss of DAXX in RSs.

On the sex chromosomes, 164 X-linked genes and 19 Y-linked genes were upregulated (Fig. 4D; Supplemental Fig. S3E), with enrichment of upregulated genes observed on the X chromosome (Fig. 4F). These upregulated genes were also enriched in regions of chromosome 14 that share epigenomic features with PMSC (Moretti et al. 2016), suggesting that postmeiotic silencing by PMSC was attenuated in *Daxx*-cKO RSs. Notably, DAXX-mediated H3.3 incorporation occurs at PSs on differentially expressed genes (DEGs) in RSs (Supplemental Fig. S3F), supporting a role for DAXX in programming gene expression. In contrast, overall expression changes of premarked gene clusters were relatively limited in *Daxx*-cKO PSs and RSs (Supplemental Fig. S3G). Despite these changes in gene expression, TE expression was only modestly altered in *Daxx*-cKO RSs at both the type and copy-number levels, and the proportion of differentially expressed TEs corresponded to their genomic distribution (Supplemental Fig. S4A–D; Supplemental Table S2). Therefore, these modest TE changes are likely secondary to alterations in gene expression. Although global TE expression dynamically changes during spermatogenesis (Sakashita et al. 2020; Otsuka et al. 2025), DAXX depletion did not cause major disruptions in TE expression during spermatogenesis (Fig. 4G).

Notably, reanalysis of published data (Erkek et al. 2013) revealed that DAXX-dependent H3.3 profiles persisted into spermatozoa, whereas H3.1/3.2 was retained at cluster 4 genes, which are not major targets of DAXX-dependent H3.3 incorporation (Fig. 4C). These findings raise the possibility that DAXX may bookmark cluster 1–3 genes in PSs, establishing an epigenetic memory that persists in spermatozoa. In contrast, both H3.1/3.2 and H3.3 were largely depleted from the sex chromosomes compared with the autosomes (Supplemental Fig. S5A), indicating that autosomes and sex chromosomes are differentially marked in sperm.

Together, these results suggest that DAXX-mediated H3.3 deposition in PSs—transcription-coupled on autosomes and DDR-dependent on the sex chromosomes during MSCI—underlies a proper epigenome in RSs, thereby regulating autosomal gene expression, maintaining postmeiotic silencing of sex-linked genes by PMSC, and possibly contributing to bookmarking the sperm epigenome (Fig. 5). These results further support the functional studies of H3.3 during spermatogenesis, which are encoded by two independent genes in the mouse genome (Yuen et al. 2014; Tang et al. 2015; Fontaine et al. 2022). Furthermore, extensive misregulation of gene expression in RSs suggests the requirement of DAXX-deposited H3.3 in the haploid program in mice, raising the possibility that many of the histone modifications on H3 detected in haploid RSs are modifications on H3.3.

Because H3.3 and its modifications in sperm are implicated in intergenerational epigenetic inheritance (Erkek

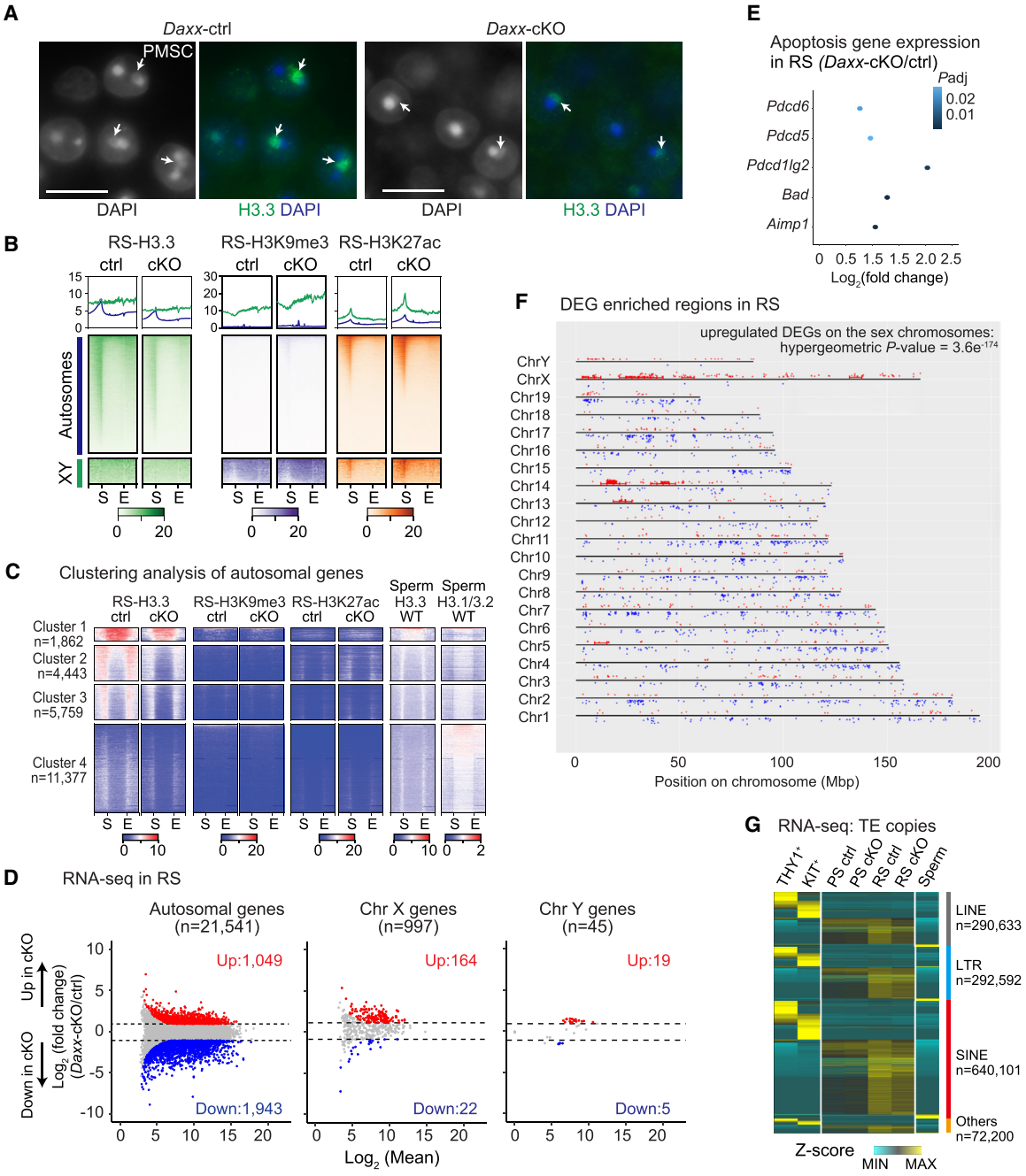

Figure 4. DAXX-mediated H3.3 deposition in PSs establishes a proper epigenome in RSs. (*A*) Immunofluorescence images of round spermatids in testicular sections. Arrows indicate postmeiotic sex chromatin (PMSC). Scale bars, 10 µm. (*B*) CUT&RUN enrichment profiles for H3.3, H3K9me3, and H3K27ac at all autosomal genes ($n = 23,441$) and all XY-linked genes ($n = 1324$). (S) TSS, (E) TES; ±3 kb from these sites. (*C*) Clustering analysis of autosomal genes in *Daxx*-ctrl and *Daxx*-cKO RSs and wild-type (WT) sperm, based on the clusters defined in Figure 3C. WT sperm H3.3 and H3.1/3.2 ChIP-seq data were reanalyzed from Erkek et al. (2013). (*D*) RNA-seq analysis of *Daxx*-ctrl and *Daxx*-cKO RSs. Differentially expressed genes (DEGs; $\log_2$ fold change > 1, adjusted $P < 0.05$) are highlighted, with numbers indicated. (*E*) Expression of apoptosis-related genes in RSs. (*F*) Chromosomal distribution of DEGs in RSs. The enrichment of upregulated DEGs on the sex chromosomes (183 XY-linked DEGs out of 1042 total XY-linked genes) is statistically significant when compared with their distribution across the entire genome (1232 upregulated DEGs out of 22,583 total genes; $P = 3.6 \times 10^{-174}$, hypergeometric test). (*G*) RNA-seq analysis of all TE copies during spermatogenesis. (THY1$^+$) Undifferentiated spermatogonia, (KIT$^+$) differentiating spermatogonia.

et al. 2013; Lismer et al. 2021; Sakashita et al. 2023), we sought to explore whether DAXX-mediated H3.3 deposition in the male germline correlates with gene expression in early embryos. Using the same gene clusters defined in Figure 3C, we found that cluster 1–3 genes display features of embryonic hypertranscription—characterized by the accumulation of the cohesin protein SMC3 (Yu et al. 2025)—by at least the 8 cell stage (Supplemental Fig. S5B). These genes were highly expressed at the 8 cell stage following zygotic genome activation at the 2 cell stage

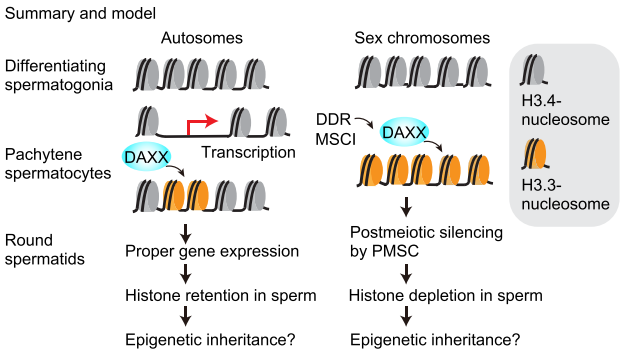

Figure 5. Summary and model of DAXX functions in the male germline. DAXX-mediated H3.3 deposition in PSs—transcription-coupled on autosomes and DDR-dependent on the sex chromosomes during MSCI—is essential for establishing a proper epigenome in RSs. This process regulates autosomal gene expression, maintains postmeiotic silencing of sex-linked genes via PMSC, and may contribute to epigenetic bookmarking in sperm.

(Supplemental Fig. S5). Although paternal H3.3 on promoters is lost after fertilization (Ishiuchi et al. 2021) and H3K27me3 is reprogrammed during preimplantation development (Zheng et al. 2016), this correlation raises the intriguing possibility that DAXX-mediated H3.3 deposition bookmarks genes for expression in early embryos. Supporting this model, a recent study suggested that paternal epigenetic memories established during MSCI persist into preimplantation development (Wei et al. 2024). Together, these findings highlight the need for further investigation into how paternal epigenetic programming influences embryonic gene expression programs.

Materials and methods

Animals

All mice were handled according to the guidelines of the Institutional Animal Care and Use Committee (IACUC: 23545) at the University of California, Davis.

Generation of Daxx*-cKO mice*

Daxx$^{flox/+}$ transgenic mice were purchased from the Jackson Laboratory (B6.129-Daxxem1Glo/J, strain no. 037960). *Ddx4-Cre*$^{Tg/+}$ transgenic mice were purchased from the Jackson Laboratory [FVB-Tg(Ddx4-cre)1Dcas/J, strain no. 006954].

Preparation of meiotic chromosome spreads

Meiotic chromosome spread preparation, immunostaining, and data analysis were performed as described previously (Alavattam et al. 2018). Histology and immunostaining were performed as described previously (Abe et al. 2022).

Isolation of pachytene spermatocytes

Isolation of pachytene spermatocytes using fluorescence-activated cell sorting (FACS) was performed using SH800S (Sony), with Vybrant DyeCycle violet-stained (Invitrogen V35003) testicular single-cell suspensions prepared as described previously (Yeh et al. 2021).

Next-generation sequencing analysis

Library generation and data analyses for RNA-seq and CUT&RUN are described in the Supplemental Material.

Other detailed experimental procedures are described in the Supplemental Material.

Code availability

Source code for all software and tools used in this study, along with documentation, examples, and additional information, are available at the URLs listed in the Supplemental Material.

Data availability

RNA-seq data and CUT&RUN data sets have been deposited in the NCBI Gene Expression Omnibus under accession code GSE308667. The accession codes for the raw published data used in this study are as follows: sperm H3.3 and H3.1/3.2 ChIP-seq (Fig. 4C; Supplemental Fig. S5A): GSE42629 (Erkek et al. 2013); E13.5 and E16.5 RNA-seq (Fig. 1B): ERP001953 (Seisenberger et al. 2012); THY1^{+}, PS, and RS RNA-seq (Figs. 1B, 4G): GSE55060 (Hasegawa et al. 2015); KIT^{+} RNA-seq (Figs. 1B, 4G): GSE89502 (Maezawa et al. 2018); sperm RNA-seq (Fig. 4G): DDBJ DRP000508 (Kobayashi et al. 2012); RNA-seq at various stages of spermatogenesis (Supplemental Fig. S3D,E): GSE107644 (Chen et al. 2018); and embryonic cohesin SMC3 CUT&RUN and RNA-seq (Supplemental Fig. S5B): GSE200323 (Yu et al. 2025).

Competing interest statement

The authors declare no competing interests.

Acknowledgments

We thank Richard M. Schultz for discussion, critical reading, and editing of the manuscript; members of the Namekawa laboratory and Neil Hunter for discussion; Yasuyuki Ohkawa for providing the anti-H3.4 antibody; Yoshinori Watanabe and Yuki Okada for providing the anti-ATF7IP2 antibody; and Mary Ann Handel for providing the anti-H1T antibody. This study was supported by National Institutes of Health (NIH) Training Program T32ES007059 and the Yen Chuang Taiwan Fellowship to Y.-H.Y., and University of California, Davis, startup funds and NIH R35 GM141085 to S.H.N.

Author contributions: Y.-H.Y. and S.H.N. designed the study. Y.-H.Y., M.H., B.M.A., S.S.N., and H.W. performed the experiments. Y.-H.Y. performed the bulk RNA-seq and CUT&RUN experiments. Y.-H.Y., M.H., K.O., S. M., and S.H.N. designed and interpreted the computational analyses. Y.-H.Y., M.H., K.O., S.M., and S.H.N.

interpreted the results. Y.-H.Y. and S.H.N. wrote the manuscript with critical feedback from all of the other authors. S.H.N. supervised the project.

References

Abe H, Yeh YH, Munakata Y, Ishiguro KI, Andreassen PR, Namekawa SH. 2022. Active DNA damage response signaling initiates and maintains meiotic sex chromosome inactivation. *Nat Commun* **13:** 7212. doi:10.1038/s41467-022-34295-5

Adams SR, Maezawa S, Alavattam KG, Abe H, Sakashita A, Shroder M, Broering TJ, Sroga Rios J, Thomas MA, Lin X, et al. 2018. RNF8 and SCML2 cooperate to regulate ubiquitination and H3K27 acetylation for escape gene activation on the sex chromosomes. *PLoS Genet* **14:** e1007233. doi:10.1371/journal.pgen.1007233

Alavattam KG, Abe H, Sakashita A, Namekawa SH. 2018. Chromosome spread analyses of meiotic sex chromosome inactivation. *Methods Mol Biol* **1861:** 113–129. doi:10.1007/978-1-4939-8766-5_10

Alavattam KG, Maezawa S, Andreassen PR, Namekawa SH. 2021. Meiotic sex chromosome inactivation and the XY body: a phase separation hypothesis. *Cell Mol Life Sci* **79:** 18. doi:10.1007/s00018-021-04075-3

Alavattam KG, Esparza JM, Hu M, Shimada R, Kohrs AR, Abe H, Munakata Y, Otsuka K, Yoshimura S, Kitamura Y, et al. 2024. ATF7IP2/MCAF2 directs H3K9 methylation and meiotic gene regulation in the male germline. *Genes Dev* **38:** 115–130. doi:10.1101/gad.351569.124

Carraro M, Hendriks IA, Hammond CM, Solis-Mezarino V, Völker-Albert M, Elsborg JD, Weisser MB, Spanos C, Montoya G, Rappsilber J, et al. 2023. DAXX adds a de novo H3.3K9me3 deposition pathway to the histone chaperone network. *Mol Cell* **83:** 1075–1092.e9. doi:10.1016/j.molcel.2023.02.009

Chen Y, Zheng Y, Gao Y, Lin Z, Yang S, Wang T, Wang Q, Xie N, Hua R, Liu M, et al. 2018. Single-cell RNA-seq uncovers dynamic processes and critical regulators in mouse spermatogenesis. *Cell Res* **28:** 879–896. doi:10.1038/s41422-018-0074-y

Choi J, Kim T, Cho EJ. 2024. HIRA vs. DAXX: the two axes shaping the histone H3.3 landscape. *Exp Mol Med* **56:** 251–263. doi:10.1038/s12276-023-01145-3

Elsässer SJ, Noh KM, Diaz N, Allis CD, Banaszynski LA. 2015. Histone H3.3 is required for endogenous retroviral element silencing in embryonic stem cells. *Nature* **522:** 240–244. doi:10.1038/nature14345

Erkek S, Hisano M, Liang CY, Gill M, Murr R, Dieker J, Schübeler D, van der Vlag J, Stadler MB, Peters AH. 2013. Molecular determinants of nucleosome retention at CpG-rich sequences in mouse spermatozoa. *Nat Struct Mol Biol* **20:** 868–875. doi:10.1038/nsmb.2599

Fontaine E, Papin C, Martinez G, Le Gras S, Nahed RA, Héry P, Buchou T, Ouararhni K, Favier B, Gautier T, et al. 2022. Dual role of histone variant H3.3B in spermatogenesis: positive regulation of piRNA transcription and implication in X-chromosome inactivation. *Nucleic Acids Res* **50:** 7350–7366. doi:10.1093/nar/gkac541

Gallardo T, Shirley L, John GB, Castrillon DH. 2007. Generation of a germ cell-specific mouse transgenic Cre line, Vasa-Cre. *Genesis* **45:** 413–417. doi:10.1002/dvg.20310

Hasegawa K, Sin HS, Maezawa S, Broering TJ, Kartashov AV, Alavattam KG, Ichijima Y, Zhang F, Bacon WC, Greis KD, et al. 2015. SCML2 establishes the male germline epigenome through regulation of histone H2A ubiquitination. *Dev Cell* **32:** 574–588. doi:10.1016/j.devcel.2015.01.014

Hirota T, Blakeley P, Sangrithi MN, Mahadevaiah SK, Encheva V, Snijders AP, ElInati E, Ojarikre OA, de Rooij DG, Niakan KK, et al. 2018. SETDB1 links the meiotic DNA damage response to sex chromosome silencing in mice. *Dev Cell* **47:** 645–659.e6. doi:10.1016/j.devcel.2018.10.004

Ishiuchi T, Abe S, Inoue K, Yeung WKA, Miki Y, Ogura A, Sasaki H. 2021. Reprogramming of the histone H3.3 landscape in the early mouse embryo. *Nat Struct Mol Biol* **28:** 38–49. doi:10.1038/s41594-020-00521-1

Kobayashi H, Sakurai T, Imai M, Takahashi N, Fukuda A, Yayoi O, Sato S, Nakabayashi K, Hata K, Sotomaru Y, et al. 2012. Contribution of intragenic DNA methylation in mouse gametic DNA methylomes to establish oocyte-specific heritable marks. *PLoS Genet* **8:** e1002440. doi:10.1371/journal.pgen.1002440

Lewis PW, Elsaesser SJ, Noh KM, Stadler SC, Allis CD. 2010. Daxx is an H3.3-specific histone chaperone and cooperates with ATRX in replication-independent chromatin assembly at telomeres. *Proc Natl Acad Sci* **107:** 14075–14080. doi:10.1073/pnas.1008850107

Li Z, Xiong C, Shen J, Tan C, Ma D, Chen J, Liu R, Sun Q, Gong W, Yuan W, et al. 2026. DAXX governs the silencing of LINE1 during spermatogenesis in mice. *Nucleic Acids Res* **54:** gkag141. doi:10.1093/nar/gkag141

Lin CJ, Koh FM, Wong P, Conti M, Ramalho-Santos M. 2014. Hira-mediated H3.3 incorporation is required for DNA replication and ribosomal RNA transcription in the mouse zygote. *Dev Cell* **30:** 268–279. doi:10.1016/j.devcel.2014.06.022

Lismer A, Dumeaux V, Lafleur C, Lambrot R, Brind'Amour J, Lorincz MC, Kimmins S. 2021. Histone H3 lysine 4 trimethylation in sperm is transmitted to the embryo and associated with diet-induced phenotypes in the offspring. *Dev Cell* **56:** 671–686.e6. doi:10.1016/j.devcel.2021.01.014

Liu Z, Tardat M, Gill ME, Royo H, Thierry R, Ozonov EA, Peters AH. 2020. SUMOylated PRC1 controls histone H3.3 deposition and genome integrity of embryonic heterochromatin. *EMBO J* **39:** e103697. doi:10.15252/embj.2019103697

Maezawa S, Hasegawa K, Yukawa M, Kubo N, Sakashita A, Alavattam KG, Sin HS, Kartashov AV, Sasaki H, Barski A, et al. 2018. Polycomb protein SCML2 facilitates H3K27me3 to establish bivalent domains in the male germline. *Proc Natl Acad Sci* **115:** 4957–4962. doi:10.1073/pnas.1804512115

Maezawa S, Sakashita A, Yukawa M, Chen X, Takahashi K, Alavattam KG, Nakata I, Weirauch MT, Barski A, Namekawa SH. 2020. Super-enhancer switching drives a burst in gene expression at the mitosis-to-meiosis transition. *Nat Struct Mol Biol* **27:** 978–988. doi:10.1038/s41594-020-0488-3

Moretti C, Vaiman D, Tores F, Cocquet J. 2016. Expression and epigenomic landscape of the sex chromosomes in mouse post-meiotic male germ cells. *Epigenetics Chromatin* **9:** 47. doi:10.1186/s13072-016-0099-8

Namekawa SH, Park PJ, Zhang LF, Shima JE, McCarrey JR, Griswold MD, Lee JT. 2006. Postmeiotic sex chromatin in the male germline of mice. *Curr Biol* **16:** 660–667. doi:10.1016/j.cub.2006.01.066

Nashun B, Hill PW, Smallwood SA, Dharmalingam G, Amouroux R, Clark SJ, Sharma V, Ndjetehe E, Pelczar P, Festenstein RJ, et al. 2015. Continuous histone replacement by Hira is essential for normal transcriptional regulation and de novo DNA methylation during mouse oogenesis. *Mol Cell* **60:** 611–625. doi:10.1016/j.molcel.2015.10.010

Otsuka K, Sakashita A, Maezawa S, Schultz RM, Namekawa SH. 2025. KRAB zinc-finger proteins regulate endogenous retroviruses to sculpt germline transcriptomes and genome evolution. *Genome Res* **35:** 417–431. doi:10.1101/gr.279924.124

Ray-Gallet D, Quivy JP, Scamps C, Martini EM, Lipinski M, Almouzni G. 2002. HIRA is critical for a nucleosome assembly pathway independent of DNA synthesis. *Mol Cell* **9:** 1091–1100. doi:10.1016/S1097-2765(02)00526-9

Rogers RS, Inselman A, Handel MA, Matunis MJ. 2004. SUMO modified proteins localize to the XY body of pachytene spermatocytes. *Chromosoma* **113:** 233–243. doi:10.1007/s00412-004-0311-7

Sakashita A, Maezawa S, Takahashi K, Alavattam KG, Yukawa M, Hu YC, Kojima S, Parrish NF, Barski A, Pavlicev M, et al. 2020. Endogenous retroviruses drive species-specific germline transcriptomes in mammals. *Nat Struct Mol Biol* **27:** 967–977. doi:10.1038/s41594-020-0487-4

Sakashita A, Ooga M, Otsuka K, Maezawa S, Takeuchi C, Wakayama S, Wakayama T, Namekawa SH. 2023. Polycomb protein SCML2 mediates paternal epigenetic inheritance through sperm chromatin. *Nucleic Acids Res* **51:** 6668–6683. doi:10.1093/nar/gkad479

Seisenberger S, Andrews S, Krueger F, Arand J, Walter J, Santos F, Popp C, Thienpont B, Dean W, Reik W. 2012. The dynamics of genome-wide DNA methylation reprogramming in mouse primordial germ cells. *Mol Cell* **48:** 849–862. doi:10.1016/j.molcel.2012.11.001

Shao Q, Zhang Y, Liu Y, Shang Y, Li S, Liu L, Wang G, Zhou X, Wang P, Gao J, et al. 2023. ATF7IP2, a meiosis-specific partner of SETDB1, is required for proper chromosome remodeling and crossover formation during spermatogenesis. *Cell Rep* **42:** 112953. doi:10.1016/j.celrep.2023.112953

Tagami H, Ray-Gallet D, Almouzni G, Nakatani Y. 2004. Histone H3.1 and H3.3 complexes mediate nucleosome assembly pathways dependent or independent of DNA synthesis. *Cell* **116:** 51–61. doi:10.1016/S0092-8674(03)01064-X

Tang MC, Jacobs SA, Mattiske DM, Soh YM, Graham AN, Tran A, Lim SL, Hudson DF, Kalitsis P, O'Bryan MK, et al. 2015. Contribution of the two genes encoding histone variant h3.3 to viability and fertility in mice. *PLoS Genet* **11:** e1004964. doi:10.1371/journal.pgen.1004964

Turner JM. 2015. Meiotic silencing in mammals. *Annu Rev Genet* **49:** 395–412. doi:10.1146/annurev-genet-112414-055145

Ueda J, Harada A, Urahama T, Machida S, Maehara K, Hada M, Makino Y, Nogami J, Horikoshi N, Osakabe A, et al. 2017. Testis-specific histone variant H3t gene is essential for entry into spermatogenesis. *Cell Rep* **18:** 593–600. doi:10.1016/j.celrep.2016.12.065

van der Heijden GW, Derijck AA, Pósfai E, Giele M, Pelczar P, Ramos L, Wansink DG, van der Vlag J, Peters AH, de Boer P. 2007. Chromosome-wide nucleosome replacement and H3.3 incorporation during mammalian meiotic sex chromosome inactivation. *Nat Genet* **39:** 251–258. doi:10.1038/ng1949

Wei C, Kesner B, Yin H, Lee JT. 2024. Imprinted X chromosome inactivation at the gamete-to-embryo transition. *Mol Cell* **84:** 1442–1459.e7. doi:10.1016/j.molcel.2024.02.013

Yeh YH, Hu M, Nakagawa T, Sakashita A, Yoshida S, Maezawa S, Namekawa SH. 2021. Isolation of murine spermatogenic cells using a violet-excited cell-permeable DNA binding dye. *J Vis Exp*. doi:10.3791/61666

Yu G, Xu K, Xia W, Zhang K, Xu Q, Li L, Lin Z, Liu L, Liu B, Du Z, et al. 2025. Establishment of chromatin architecture interplays with embryo hypertranscription. *Nature* **646:** 208–217. doi:10.1038/s41586-025-09400-5

Yuen BT, Bush KM, Barrilleaux BL, Cotterman R, Knoepfler PS. 2014. Histone H3.3 regulates dynamic chromatin states during spermatogenesis. *Development* **141:** 3483–3494. doi:10.1242/dev.106450

Zheng H, Huang B, Zhang B, Xiang Y, Du Z, Xu Q, Li Y, Wang Q, Ma J, Peng X, et al. 2016. Resetting epigenetic memory by reprogramming of histone modifications in mammals. *Mol Cell* **63:** 1066–1079. doi:10.1016/j.molcel.2016.08.032